ACS NANOSCIENCE Au
AN OPEN ACCESS JOURNAL OF THE AMERICAN CHEMICAL SOCIETY

pubs.acs.org/nanoau
Article

Synergistic Effects of ZnO@NiM′-Layered Double Hydroxide (M′ = Mn, Co, and Fe) Composites on Supercapacitor Performance: A Comparative Evaluation

Published as part of ACS Nanoscience Auspecial issue"Advances in Energy Conversion and Storage at the Nanoscale".

Gaurav Pandey,[†] Surendra Serawat,[†] and Kamlendra Awasthi*

Cite This: *ACS Nanosci. Au* 2024, 4, 399−408

Read Online

ACCESS | Metrics & More | Article Recommendations | Supporting Information

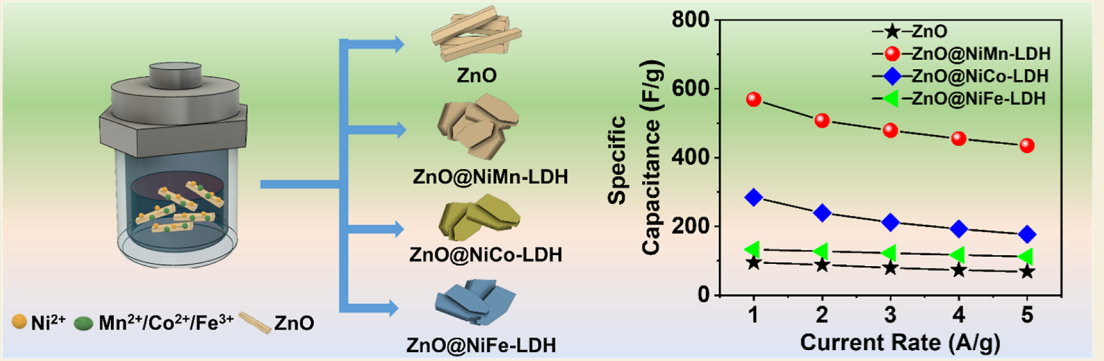

ABSTRACT: The development of supercapacitors is pivotal for sustainable energy storage solutions, necessitating the advancement of innovative electrode materials to supplant fossil-fuel-based energy sources. Zinc oxide (ZnO) is widely studied for use in supercapacitor electrodes because of its beneficial physicochemical properties, including excellent chemical and thermal stability, semiconducting characteristics, low cost, and environmentally friendly nature. In this study, ZnO nanorods were synthesized using a simple hydrothermal method and then combined with various Ni-based layered double hydroxides (LDHs) [NiM′-LDHs (M′ = Mn, Co, and Fe)] to improve the electrochemical performance of the ZnO nanorods. These LDHs are well-known for their outstanding electrochemical and electronic properties, high specific capacitance, and efficient dispersion of cations within host nanolayers. The synthesized composites ZnO@NiMn-LDH, ZnO@NiCo-LDH, and ZnO@NiFe-LDH exhibit enhanced specific capacitances of 569.3, 284.6, and 133.0 F/g, respectively, at a current rate of 1 A/g, outperforming bare ZnO (98.4 F/g). Notably, ZnO@NiMn-LDH demonstrates superior electrochemical performance along with a capacitance retention of 76%, compared to ZnO@NiCo-LDH (58%), ZnO@NiFe-LDH (49%), and bare ZnO (23%) over 5000 cycles. Furthermore, an asymmetric supercapacitor (ASC) was developed by using ZnO@NiMn-LDH as the positive electrode and activated carbon (AC) as the negative electrode to assess its practical applicability. The fabricated ASC (ZnO@NiMn-LDH//AC) demonstrated a specific capacitance of 45.22 F/g at a current rate of 1 A/g, an energy density of 16.08 W h/kg at a power density of 798.8 W/kg, and a capacitance retention of 75% over 5000 cycles. These findings underscore the potential of the composite formation of ZnO with Ni-based LDHs in advancing the efficiency and durability of supercapacitors.

KEYWORDS: *ZnO composites, hydrothermal, layered double hydroxides, supercapacitor, nickel-based LDHs*

1. INTRODUCTION

Excessive environmental pollution from greenhouse gas emissions associated with fossil fuel consumption necessitates urgent development of energy conversion and storage systems.[1] Presently, batteries, especially lithium-ion batteries, are meeting current energy demands due to their high energy density and portability. However, the relatively low power density of existing battery technologies limits their broader application potential.[2] In contrast, supercapacitors offer

Received: June 14, 2024
Revised: September 3, 2024
Accepted: September 4, 2024
Published: September 16, 2024

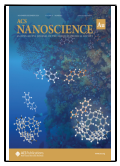

https://doi.org/10.1021/acsnanoscienceau.4c00029
ACS Nanosci. Au 2024, 4, 399−408

significantly higher power density compared to conventional batteries, making them a promising alternative.[3−7] Supercapacitors are categorized into electric double-layer capacitors (EDLCs) and pseudocapacitors based on their charge storage mechanism.[8−10] Generally, EDLCs are carbonaceous materials that store the charge due to surface adsorption and desorption at the electrode/electrolyte interface, while transition metal compounds and conducting polymers are pseudocapacitive type electrode materials. Generally, pseudocapacitors, in particular, rely on reversible Faradaic redox reactions, which enable higher specific capacitance and energy density compared to EDLCs.[11,12] Ruthenium oxide (RuO_2) is the initial metal oxide explored for supercapacitor materials due to their high specific capacitance; however, its toxicity and high cost limited its application in the field of supercapacitors.[13] Various other inexpensive and low toxic metal oxides, such as ZnO,[14] NiO,[15] MnO_2,[16] Co_3O_4,[17] etc., were explored for supercapacitor applications due to their stability and enhanced electrochemical properties.

Zinc oxide (ZnO), a metal oxide semiconductor having a band gap of 3.37 eV, is widely explored in various fields of applications such as electronics, sensors, optics, optoelectronics, solar cells, photocatalysis, etc.[18−22] The low cost, ease of production, high thermal and chemical stability, abundant nature, and environmental friendliness of ZnO make it a suitable choice for a wide range of applications.[23] In the field of energy storage applications, ZnO is used as an electrode material for high energy density applications such as alkali (Li^+, Na^+, and K^+) ion batteries.[24−28] In the case of the supercapacitor, Luo et al. investigated the supercapacitive characteristics of ZnO tetrapods synthesized through oxidative−metal−vapor−transport methods, which delivers a specific capacitance of 160.4 F/g at 1 A/g.[14] In another work, Shaheen et al. synthesized the ZnO nanoparticles using organic fuels, which deliver the specific capacitance of 86 F/g at 2 mV/s.[29] The inherent lower conductivity of ZnO remains a bottleneck for achieving high-performance supercapacitors, leading to reduced specific capacitances and poor cyclic stability.[30] This leads researchers to do various modifications with ZnO, such as doping with different transition metals (Co,[31] Ni,[32] Fe,[33] Mo,[34] etc.), carbon coating (graphene,[35] carbon, rGO,[36,37] etc.), and composite formation with metal oxides (Co_3O_4, MnO_2,[38] CuO,[37] NiO[39]) and hydroxide ($Ni(OH)_2$,[40]). For example, Shaheen et al. utilize the composite formation of ZnO−Co_3O_4, which showed a specific capacitance of 165.4 F/g at 2 mV/s.[41] Another work done by Shaheen et al. reported the composite formation of ZnO with Pd/PdO using hydrothermal methods, which, upon modification, was able to deliver a specific capacitance of 178 F/g at a scan rate of 2 mV/s.[42] Furthermore, Pang et al. synthesized ZnO−NiO micropolyhedra by calcinating mixed oxalate ($Zn_{0.9}Ni_{0.1}(C_2O_4)_2{\cdot}nH_2O$) at various temperatures. The synergistic effect of these metal oxides yielded a specific capacitance of 649.0 F/g at 5.8 A/g and retained 99.1% of its specific capacitance after 400 cycles at the same current rate.[43]

In addition to being modified with other metal oxides, layered double hydroxides (LDHs) have recently emerged as a suitable option for composite formation. This is because of their outstanding electrochemical and electronic properties, stemming from their flexible structure, high specific capacitance value, and effective dispersion of cations within the host nanolayers.[44] LDHs are hydrotalcite-like compounds or anionic clays having the structure $[M^{2+}_{1-x}M^{3+}_x(OH)_2]$-$A^{n-}{}_{x/n}{\cdot}mH_2O$ (M^{2+}, and M^{3+} are the bivalent ions, i.e. Ni^{2+}, Mg^{2+}, Ca^{2+}, etc. and, trivalent metal cations, i.e. Co^{3+}, Fe^{3+}, Mn^{3+}, Al^{3+}, etc., and A^{n-} is the sandwich anion, i.e. Cl^-, $NO_3{}^{2-}$, $Co_3{}^{2-}$, etc.).[45] Among them, Ni-based LDHs are quite an appealing candidate for electrochemical application due to nickel's low cost, environmental friendliness, and high theoretical capacitance value.[46] Various Ni-based LDHs, such as NiMn-LDHs,[10] NiCo-LDHs,[47] and NiFe-LDHs,[48] were explored as electrode material for supercapacitor application due to high redox activity, synergistic effect of bimetallic ions, intercalating capability, and outstanding electrochemical performance. The LDHs not only charge via layered type structure but also store due to the multiple oxidation states of the surface elements.[44] However, a challenge with present LDHs is the accumulation of their layered structure over cycling, leading to poor electrical conductivity and charge transport, consequently blocking active sites.[44]

The composite formation of metal oxides with Ni-based LDH is quietly explored as a remedial approach for enhancing the overall electrochemical performance due to the synergistic effect. Xiong et al. synthesized NiCo-LDH/ZnO/CC by taking the ZnO nanoflowers with NiCo-LDH nanoflakes. Incorporating both materials results in higher electrochemical performance compared to ZnO-based supercapacitors.[49] Chen et al. conducted similar research, demonstrating that the composite formation of NiCo-LDH with ZnO nanorods achieved a high areal capacitance of 667.3 mF/cm^2 at 1 mA/cm^2. Additionally, it exhibited cyclic stability of 86.78% over 2000 cycles, surpassing the performance of bare ZnO and NiCo-LDH materials.[50]

From the above discussion, it is evident that the composite formation of ZnO with LDHs enhances the electrochemical performance of ZnO. Therefore, our approach involved initially synthesizing ZnO nanostructures through a straightforward hydrothermal method. This method was preferred over other synthesis techniques such as sol−gel,[51] solid-state,[52] and spray pyrolysis[53] due to its numerous advantages, including cost-effectiveness, one-step process, high safety, and its ability to precisely control the morphology of the synthesized materials. Subsequently, we synthesized composites by employing various NiM′-LDHs (M′ = Mn, Co, and Fe) using the same hydrothermal technique. Notably, our synthesized ZnO@NiMn-LDH composite demonstrated superior performance compared to other compositions, boasting a specific capacitance of 569.3 F/g at 1 A/g while retaining 76% capacitance after 5000 cycles. The comprehensive electrochemical measurements and insights into the charge-storage mechanism of ZnO@NiMn-LDH are thoroughly discussed. Moreover, we assembled an asymmetric supercapacitor (ASC), which exhibited an energy density of 16.08 W h/kg at a power density of 798.8 W/kg, maintaining a cyclic stability of 75% over 5000 cycles.

2. EXPERIMENTAL SECTION

2.1. Materials

Nickel sulfate hexahydrate ($NiSO_4{\cdot}6H_2O$, 99%, CDH, India), manganese sulfate monohydrate ($MnSO_4{\cdot}H_2O$, 99%, Fisher, USA), cobalt nitrate hexahydrate ($Co(NO_3)_2{\cdot}6H_2O$, ≥98%, Sigma-Aldrich, USA), iron nitrate nonahydrate ($Fe(NO_3)_3{\cdot}9H_2O$, ≥98%, Sigma-Aldrich, USA), zinc nitrate hexahydrate ($Zn(NO_3)_2{\cdot}6H_2O$, 98%, Loba Chemie, India), hexamethyltetramine ($C_6H_{12}N_4$, HMTA, 99%, Merck, USA), and urea (CH_4N_2O, 99.5%, CDH, India) were used as the precursor for the synthesis. Deionized (DI) water and ethanol

https://doi.org/10.1021/acsnanoscienceau.4c00029
ACS Nanosci. Au 2024, 4, 399−408

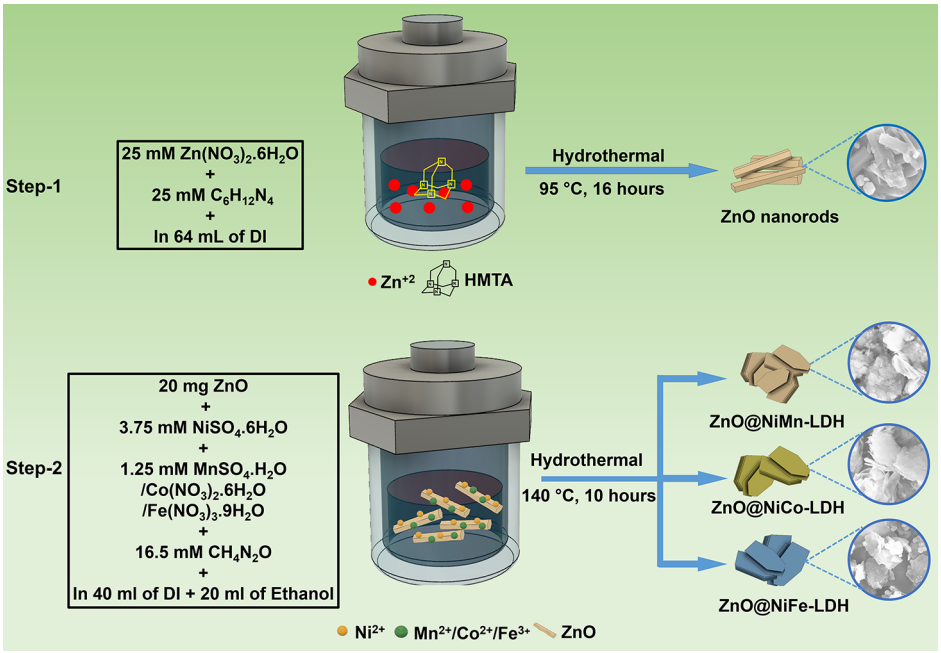

Figure 1. Schematic representation of the hydrothermal synthesis of ZnO and ZnO@NiM′-LDHs (M′ = Mn, Co, and Fe).

(99%) were used as solvents. Ni foam (99%), supplied by Kanopy Pvt. Ltd., India, was used as the substrate for the working electrode. Super-P (C, 99+%, Alfa Aesar, USA) and polyvinylidene fluoride (PVDF, Sigma-Aldrich, USA) were used as the conducting agent and binder in the working electrode preparation. *N*-Methyl-2-pyrrolidone (NMP, 99%+, Alfa Aesar, USA) was used as the solvent for the slurry preparation of the electrode. Potassium hydroxide (KOH, 85.0%, CDH, India) was used for the preparation of electrolyte.

2.2. Material Preparation

2.2.1. Synthesis of ZnO. A typical hydrothermal method was employed for the synthesis of ZnO. In this process, 25 mM $Zn(NO_3)_2{\cdot}6H_2O$ was mixed with an equimolar amount of HMTA in 64 mL of DI water. After thorough mixing, the solution was transferred to a Teflon-lined autoclave and placed in an oven at 95 °C for 16 h. Upon completion of the reaction, the product was collected by centrifugation and washed three times with DI water and ethanol. The final product was then dried at 60 °C for 10 h.

2.2.2. Synthesis of ZnO@NiM′-LDHs (M′ = Mn, Co, and Fe). For the synthesis of ZnO@NiMn-LDH, 20 mg of synthesized ZnO was added to a mixture of 40 mL of DI water and 20 mL of ethanol. Then, 3.75 mmol of $NiSO_4{\cdot}6H_2O$, 1.25 mmol of $MnSO_4{\cdot}H_2O$, and 16.5 mmol of urea were added to the solution. After thorough mixing, the solution was placed in a Teflon-lined autoclave and heated in an oven at 140 °C for 10 h. Upon completion of the reaction, the product was collected by centrifugation and washed three times with DI water and ethanol, followed by drying at 60 °C for 5 h. For the synthesis of ZnO@NiCo-LDH and ZnO@NiFe-LDH, 1.25 mmol of the Mn precursor was replaced with 1.25 mmol of the cobalt precursor ($Co(NO_3)_2{\cdot}6H_2O$) and 1.25 mmol of Fe precursors ($Fe(NO_3)_3{\cdot}9H_2O$), respectively. The graphical depiction of the overall synthesis of ZnO and ZnO@NiM′-LDH is shown in Figure 1.

2.3. Material Characterization

The phase formation of synthesized material was confirmed by using the X-ray diffraction method (Panalytical X'Pert Pro X-ray diffractometer) using Cu−Kα_1 (λ = 0.154 nm) as the source. The morphology of the synthesized material was characterized using a scanning electron microscope coupled with EDS (FESEM, SSPRA 40 VP, Zeiss) and a transmission electron microscope (HRTEM, FEI-Titan G^2 60−300 kV). For the determination of the oxidation state of the constituent element in the synthesized material, X-ray spectroscopy (ESCA$^+$ Omicron nanotechnology spectrometer, Al K_α-source, 1486.7 eV) was used. For the determination of Brunauer−Emmett−Teller (BET) surface area and BJH adsorption−desorption measurements, a BET surface area analyzer (Quanta chrome Nova Touch LX2) was used.

2.4. Electrochemical Measurements

The electrochemical measurements of the synthesized material were conducted by using an electrochemical workstation (Squidstat Plus, Admiral Instruments, USA) in both three-electrode and two-electrode configurations. The working electrode was prepared by mixing the synthesized material (ZnO@NiM′-LDH) with Super-P and PVDF in a mortar and pestle at a weight ratio of 8:1:1. A viscous slurry was then prepared by adding a few drops of NMP. The obtained slurry was coated on Ni foam and dried at 60 °C for 12 h. The mass of the electrode materials was obtained by subtracting the bare mass of the Ni foam. The active mass of the electrode was approximately 1.18−1.28 mg for all combinations of material. In the three-electrode configuration, the material-coated Ni foam was used as the working electrode, platinum (Pt) mesh was used as the counter electrode, and a saturated calomel electrode (Hg/HgO (saturated 1 M KOH)) was used as the reference electrode. A 6 M KOH aqueous solution was used as the electrolyte. Cyclic voltammetry (CV) and galvanostatic charge−discharge (GCD) measurements were conducted, and the specific capacitance (in F/g) was calculated from the discharge time obtained from the GCD measurement using the following equations

$$C_s = \frac{i \times \Delta t}{m \times \Delta V} \tag{1}$$

where i is the current (in amp), m is the mass of active material (in gram), ΔV is the working potential window (in volts), and Δt is the discharge time (in sec).

Further, the electrical characterization of the fabricated electrode materials was performed using electrochemical impedance spectroscopy (EIS) with an activated carbon (AC) amplitude of 5 mV in the frequency range of 0.1 Hz to 1 MHz. For the assembly of the ASC, a similar negative electrode on Ni foam was prepared by using AC, Super-P, and PVDF. The ZnO@NiMn-LDH on Ni foam served as the positive electrode, separated by a separator, with 6 M KOH as the electrolyte. The electrochemical measurements were performed in a two-electrode configuration. The mass loading of both the positive and negative electrode materials was balanced using the following equation

https://doi.org/10.1021/acsnanoscienceau.4c00029
ACS Nanosci. Au 2024, 4, 399−408

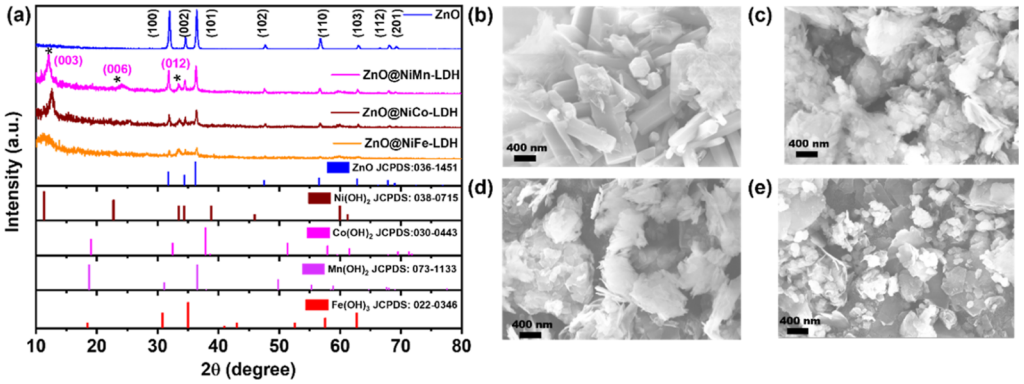

Figure 2. (a) XRD pattern of the as-synthesized ZnO@NiM′-LDHs (M′ = Mn, Co, and Fe), FESEM image of (b) ZnO, (c) ZnO@NiMn-LDH, (d) ZnO@NiCo-LDH, and (e) ZnO@NiFe-LDH.

$$m_+ \times \Delta V_+ \times C_+ = m_- \times \Delta V_- \times C_- \quad (2)$$

where m, C, and ΔV represent the mass of active materials (in g), specific capacitance (F/g), and working potential window (in V) of the constituent electrode materials. The energy density (E, W h/kg) and power density (P, W/kg) of the fabricated ASC were calculated using the discharge time from the GCD and the delivered specific capacitance of the device (C_s) using the following equation

$$E = \frac{1}{2 \times 3.6} \times C_s \times \Delta V^2 \quad (3)$$

$$P = \frac{3.6 \times 1000 \times E}{\Delta t} \quad (4)$$

3. RESULTS AND DISCUSSIONS

3.1. Structural and Morphological Characterization

The XRD patterns of synthesized ZnO and ZnO@NiM′-LDHs (M′ = Mn, Co, and Fe) are shown in Figure 2a. The characteristics peak for ZnO observed at 31.94, 34.58, 36.41, and 56.75° can be ascribed to the (100), (002), (101), and (110) planes of ZnO and matches with a hexagonal wurtzite crystal structure of ZnO (JCPDS: 0036-1451).[54] The absence of any additional peaks confirms the purity of the synthesized ZnO, and the sharp nature of the peak indicates the high crystallinity of ZnO. The XRD spectra of ZnO@NiM′-LDHs (M′ = Mn, Co, and Fe) comprised the combination of characteristics peak of both ZnO and α-Ni(OH)$_2$. The diffraction peaks at 11.99, 24.08, and 33.38° for ZnO@NiMn-LDH can be ascribed to the (003), (006), and (012) planes of the brucite structure with the hexagonal crystal phase of α-Ni(OH)$_2$ (JCPDS: 38-0715).[55] Similar kinds of peak positions were observed for ZnO@NiCo-LDH and ZnO@NiFe-LDH, with slight shifting in the peak position due to the introduction of different ions (Co and Fe). The morphological characterization of synthesized ZnO and ZnO@NiM′-LDH was done using FESEM. The FESEM image of ZnO shown in Figure 2b demonstrate the hexagonal nanorod-type nanostructure. After making a composite of ZnO with NiMn-LDH, NiCo-LDH, and NiFe-LDH, a typical sheet-like morphology covering the ZnO nanorods is observed for all the combinations, as shown in Figure 2c−e. To evaluate the elemental distribution within the composite, elemental distribution mapping and EDS spectra were conducted on a small area of ZnO@NiMn-LDH, as shown in Figure S1. The results demonstrate that Ni, Mn, Zn, and O are well-intermixed, indicating successful composite formation. Further confirmation was obtained through TEM image and SAED pattern of ZnO@NiMn-LDH. As depicted in Figure S2a, the TEM image reveal a typical sheet-like nanostructure, consistent with FESEM observations. The SAED pattern in Figure S2b displays bright, circular concentric rings, indicating the polycrystalline nature of the composite. Further, these rings can be indexed to the (101) plane of ZnO and the (110) plane of NiMn-LDH, confirming the composite nature of the material.[56,57]

For the determination of the chemical composition and chemical bonding states within ZnO@NiMn-LDH, the sample was characterized via XPS, as shown in Figure 3. The Ni 2p spectra shown in Figure 3a comprised two peaks: Ni 2p$_{3/2}$ located at 855.4 eV and Ni 2p$_{1/2}$ located at 873.3 eV along with their satellite peak at 861.5 and 879.9 eV, which illustrates

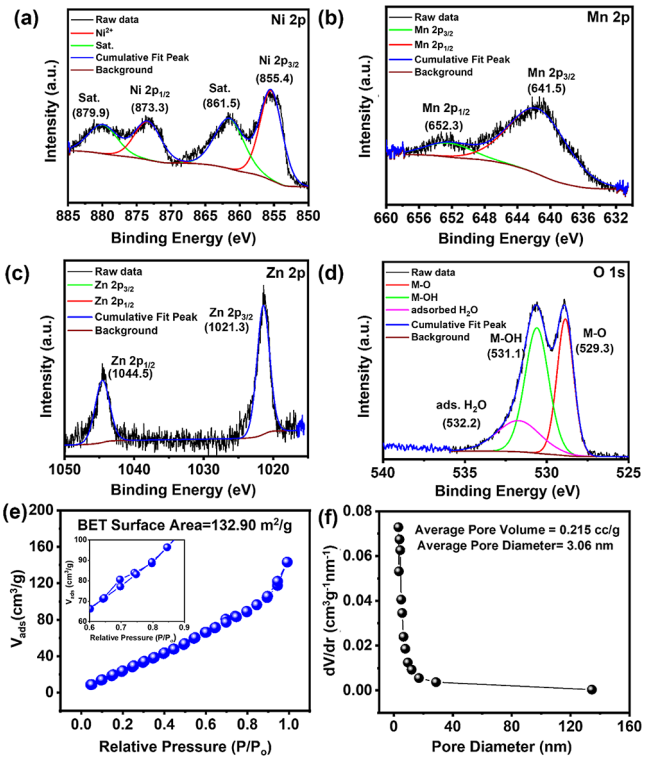

Figure 3. XPS spectra of the ZnO@NiMn-LDH for (a) Ni 2p, (b) Mn 2p, (c) Zn 2p, and (d) O 1s, (e) N_2 adsorption/desorption isotherm, and (f) pore diameter distribution of ZnO@NiMn-LDH.

https://doi.org/10.1021/acsnanoscienceau.4c00029
ACS Nanosci. Au 2024, 4, 399−408

the presence of Ni^{2+} in the ZnO@NiMn-LDH.[58] The Mn 2p spectra shown in Figure 3b show the presence of two peaks: Mn $2p_{3/2}$ located at 641.5 eV and Mn $2p_{1/2}$ located at 652.3 eV, suggesting the presence of Mn^{3+} oxidation state in the sample.[58] The presence of Mn^{3+} can be correlated as the chances of transformation from Mn^{2+} to Mn^{3+} are highly convenient due to the low redox potentials and air oxidation.[58] The Zn 2p spectra shown in Figure 3c comprised of two distinct peaks located at 1021.3 and 1044.5 eV, which correspond to the Zn $2p_{3/2}$ and Zn $2p_{1/2}$, respectively, and suggest the presence of Zn^{2+}.[54,59] In the last, the peaks for O 1s spectra shown in Figure 3d can be fitted into three distinct peaks located at 529.3, 531.1, and 532.2 eV, which can be assigned to the formation of metal oxide bond, metal hydroxide bond, and surface adsorbed hydroxyl molecule.[38,60−63] The specific surface area and pore size distribution of electrode material are very essential for energy storage application. Hence, the N_2 adsorption/desorption curve and pore size distribution of ZnO@NiMn-LDH were measured. The N_2 adsorption/desorption curve shown in Figure 3e shows the typical IV isotherms suggesting the mesoporous nature of the synthesized electrode materials with a surface area of 132.90 m^2/g. The pore size distribution curve shown in Figure 3f gives the average pore volume of 0.215 cc/g and average pore diameter of 3.06 nm, respectively.

3.2. Electrochemical Characterization

The electrochemical performance of ZnO and ZnO@NiM′-LDHs (M′ = Mn, Co, and Fe) was evaluated using CV and GCD methods in a 6 M KOH electrolyte. Comparative CV cycles at a scan rate of 50 mV/s for all samples within the potential range of 0−0.47 V are depicted in Figure 4a. The CV scans of all synthesized samples exhibit well-defined redox peaks, indicative of typical faradaic pseudocapacitive behavior.[64] Notably, the ZnO@NiMn-LDH sample displayed the largest absolute CV area, suggesting superior electrochemical activity compared to that of the other synthesized samples. Consequently, ZnO@NiMn-LDH was selected as the optimized electrode composition due to its enhanced electrochemical performance. Further, the CV and GCD measurement of ZnO@NiMn-LDH was taken at different scan rates and current rates, as shown in Figure 4b,c. The observed redox in ZnO@NiMn-LDH corresponds to the reversible reaction of Ni^{2+}/Ni^{3+}, Mn^{2+}/Mn^{3+}, and Mn^{3+}/Mn^{4+} with OH^-. The possible redox reaction can be represented via the following equations[55,58]

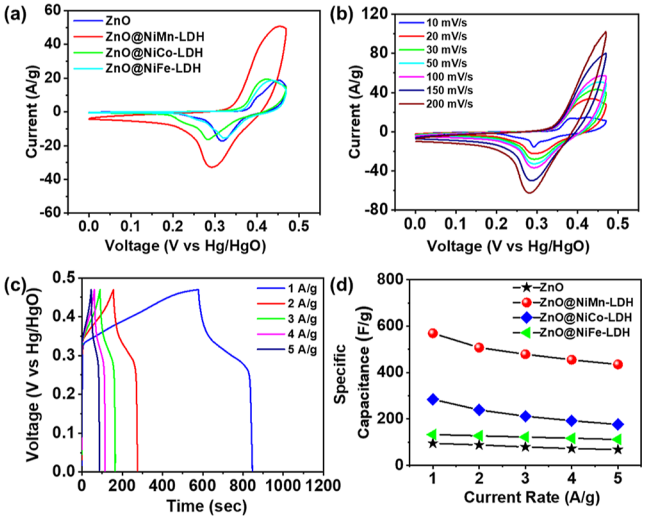

Figure 4. CV comparison graph for ZnO and ZnO@NiM′-ZnO (M′ = Mn, Co, and Fe) at a scan rate of 50 mV/s, (b) CV scan of ZnO@NiMn-LDH at different scan rates (10−200 mV/s), (c) GCD profile of ZnO@NiMn-LDH at different current rates (1−5 A/g), and (d) compared specific capacitance variation for ZnO and ZnO@NiM′-LDH (M′ = Mn, Co, and Fe) at different current rates.

$$Ni(OH)_2 + OH^- \leftrightarrow NiOOH + H_2O + e^- \quad (5)$$

$$Mn(OH)_2 + OH^- \leftrightarrow MnOOH + H_2O + e^- \quad (6)$$

$$MnOOH + OH^- \leftrightarrow MnO_2 + H_2O + e^- \quad (7)$$

The GCD profile of ZnO@NiMn-LDH at various scan rates (1−5 A/g) displays a nonlinear curve with a discharge plateau, indicating the occurrence of Faradaic reactions at the interface between the electrode materials and the alkaline electrolyte solution.[65] Notably, the Coulombic efficiency of ZnO@NiMn-LDH, derived from GCD measurements, is relatively low at 46.2% when the current rate is 1 A/g. However, it improves significantly to 90.1% as the current rate increases to 5 A/g. The low Coulombic efficiency at the lower current rate can be attributed to the presence of irreversible Faradaic reactions between the surface functionalities and the electrolyte.[67] The specific capacitance of the ZnO and ZnO@NiM′-LDH electrode materials, calculated from the discharge time, is shown in Figure 4d. The ZnO@NiMn-LDH delivers a specific capacitance of 569.3 F/g at a current rate of 1 A/g, which decreases to 434.8 F/g as the current rate increases to 5 A/g. This specific capacitance is significantly higher than that of bare ZnO (5.9 times), ZnO@NiCo-LDH (2 times), and ZnO@NiFe-LDH (by 4.2 times). This enhanced specific capacitance can be attributed to the multiple redox state of Mn compared to the Co, and Fe. The observed decrease in specific capacitance with increasing current rate is attributed to the reduced involvement of ions in redox reactions at higher current rates, resulting in lower capacitance.[66]

Further, the charge storage contribution in ZnO@NiMn-LDH was analyzed using the CV test. The relationship between the peak current (i) and the scan rate (ν) is as follows

$$i = a\nu^b \quad (8)$$

where a and b are the adjustable parameters. The value of b can be obtained from the slope of the graph between Log i vs Log ν. The value of b reflects the nature of the charge storage mechanism present in the electrode materials. For b = 0.5, it suggests domination of the diffusion-controlled process, whereas b = 1 represents the surface-controlled process.[68,69] In the case of ZnO@NiMn-LDH, the value of b lies at 0.29 and 0.31, as shown in Figure 5a, suggesting the dominance of diffusion-controlled process within the electrode materials.[57] For the determination of the percentage contribution of both charge storage mechanisms, the obtained CV current can be further decoupled according to the equation

$$i = a_1\nu + a_2\nu^{1/2} \quad (9)$$

where, $a_1\nu$ and $a_2\nu^{1/2}$ are the contribution from capacitive-controlled and diffusion-controlled current, respectively. The value of a_1 and a_2 can be obtained from the slope and intercept of the graph between $i/\nu^{1/2}$ vs $\nu^{1/2}$.[70] The contributions of both capacitance mechanisms are illustrated in Figure 5b. At lower scan rates, the diffusion-controlled process predom-

https://doi.org/10.1021/acsnanoscienceau.4c00029
ACS Nanosci. Au 2024, 4, 399−408

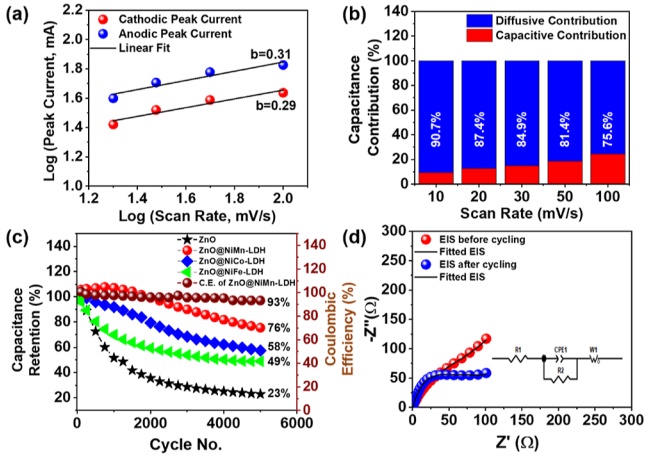

Figure 5. (a) Obtained b values from the relationship between peak current and scan rate for ZnO@NiMn-LDH, (b) contribution ratio of diffusion and capacitive controlled processes in ZnO@NiMn-LDH, (c) capacitance retention curves for all ZnO@NiM′-LDH samples at a scan rate of 100 mV/s over 5000 cycles, including the Coulombic efficiency of ZnO@NiMn-LDH, and (d) EIS measurement of ZnO@NiMn-LDH before and after cycling fitted with an equivalent circuit shown in the inset.

inates, accounting for 90.7% of the total current at a scan rate of 10 mV/s. As the scan rate increases, the contribution from the diffusion-controlled process decreases to 75.6% at a scan rate of 100 mV/s, while the contribution from the capacitive process increases. This shift occurs because, at higher scan rates, only the outer surface of the electrode material is accessible to the ions, allowing less time for the faradaic reactions to occur, hence reducing the diffusion contribution.[70]

The cyclic stability of electrode materials is a crucial factor in their practical application. The capacitance retention of the synthesized electrode materials was tested at a scan rate of 100 mV/s over 5000 cycles, as shown in Figure 5c. The ZnO@NiMn-LDH composite significantly improved overall cyclic stability, achieving a capacitance retention of 76% compared to 26% for bare ZnO, while maintaining a Coulombic efficiency of 93% over 5000 cycles, as obtained from the CV curve. In comparison, ZnO@NiCo-LDH and ZnO@NiFe-LDH demonstrated cyclic stabilities of 58% and 49%, respectively. To assess structural stability, postcycling XRD analysis of the optimized ZnO@NiMn-LDH composition cycled in a 6 M KOH electrolyte solution was conducted. The XRD spectra, shown in Figure S3, revealed prominent peaks corresponding to $Ni(OH)_2$, along with minor peaks related to ZnO. This indicates that the ZnO@NiMn-LDH structure remains stable even after cycling in a 6 M KOH solution. However, the decreased intensity of the ZnO peaks suggests the formation of an additional $Ni(OH)_2$ layer. Additionally, EIS measurements were conducted before and after cycling to gain detailed insights into the electrode materials. The resulting Nyquist spectra, shown in Figure 5d, were fitted with an equivalent circuit model. This circuit comprised resistors (R_1, R_2), a constant phase element (CPE_1), and a Warburg element (W_1). The combined electronic resistance, which includes the ohmic resistance of the electrolyte and the interfacial resistance between the current collector and electrode, is represented by R_1 and can be estimated from the high-frequency intercept of the Nyquist plot. R_2 represents the charge-transfer resistance, calculated from the diameter of the observed semicircle. The Warburg element and the constant phase element represent the diffusion of charges within the electrolyte and at the electrode/electrolyte interface, respectively.[70] The low value of R_1 (0.50 Ω) indicates the high electrical conductivity of ZnO@NiMn-LDH. The increase in charge transfer resistance from 123.4 to 142.8 Ω over 5000 cycles led to a minimal capacitance loss, as observed in Figure 5c, which is a smaller change compared to other compositions.

For the practical application of the as-synthesized ZnO@NiMn-LDH, an ASC was assembled by employing the ZnO@NiMn-LDH as the positive electrode and AC as a negative electrode. The advantage of using an ASC is its wide operating potential range, which leverages the potential windows of both the positive and negative electrodes. This leads to an increase in the overall energy density of the device, as energy density is proportional to the square of the potential window ($E = 1/2\ CV^2$).[71] The typical CV curve of a fabricated ACS is shown in Figure 6a, which is a nonrectangular shape in nature and

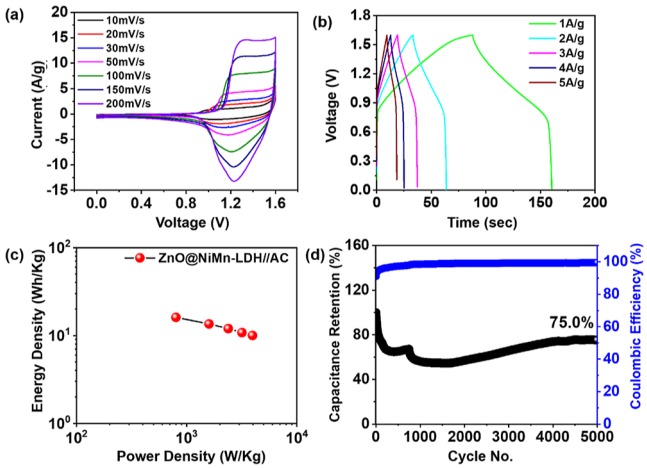

Figure 6. (a) CV curve at different scan rates (10−200 mV/s), (b) GCD profile at different current rates (1−5 A/g), (c) Ragone plot, and (d) capacitance retention at 5 A/g for 5000 cycles for ZnO@NiMn-LDH//AC ASC.

implies the coexistence of both double-layer type capacitance and pseudocapacitance. The shape of the obtained CV curve maintains at the higher scan rate, which implies good reversibility and a fast charge transfer rate.[55,68] The GCD profile of fabricated ASC at different current rates is shown in Figure 6b, which shows nonlinear and nearly symmetrical features representing good capacitive behavior.[68] The as-fabricated ASC delivers a specific capacitance of 45.22 F/g at a current rate of 1 A/g, as shown in Figure S4, and retains 62.1% of its initial capacitance when the current rate is increased from 1 to 5 A/g. The energy density (E, W h/kg) and power density (P, W/kg) are the two important key indicators in the practical application, also known as the Ragone plot of the device, as shown in Figure 6c. The as-fabricated ASC delivers a maximum energy density of 16.08 W h/kg at the power density of 798.8 W/kg and can deliver energy density up to 10.0 W h/kg at the maximum power density of 3955.6 W/kg. Further, the cyclic stability of the as-fabricated ASC was tested over 5000 cycles at a current rate of 5 A/g as shown in Figure 6d, which showed a capacitance retention of 75.0% and Coulombic efficiency close to 100%, indicating the good cycling performance of the ZnO@NiMn-LDH//AC device. The initial decrease and increase in capacitance during cycling

https://doi.org/10.1021/acsnanoscienceau.4c00029
ACS Nanosci. Au 2024, 4, 399−408

Table 1. Electrochemical Performance of Previously Reported ZnO and Ni-Based LDHs Electrodes

materials	electrolyte	specific capacitance@rate	capacitance retention@current rate	cycles	ASC Energy density@power density	ref.
ZnO	3 M KOH	86 F/g@2 mV/s			1.9 W h/kg	42
ZnO@PdO/Pd	3 M KOH	178 F/g@2 mV/s			3.3 W h/kg	42
ZnO@Co_3O_4	3 M KOH	165 F/g@2 mV/s			4.1 W h/kg@7.5 kW/kg	41
ZnO@CNT	1 M Na_2SO_4	189 F/g@1 mV/s	96%	1000 cycles		73
ZnO	2 M KOH	448 F/g@0.25 A/g	98.2%@0.5 A/g	5000 cycles		74
ZnO	1 M Na_2SO_4	160.4 F/g@1 A/g			22.3 W h/kg at 0.56 kW/kg	14
ZnO-graphene	1 M Na_2SO_4	122.4 F/g@5 mV/s				36
ZnO-rGO	0.5 M H_2SO_4	345 F/g@5 mV/s	87% after@0.5 A/g	1000 cycles		75
Cu-doped ZnO	6 M KOH	503.03 F/g@1 A/g				76
ZnO-CNT@Fe_3O_4/NF	1 M KOH	532 F/g@10 mV/s	88%@8 A/g	3000 cycles		77
ZnO−NiO	3 M KOH	649.0 F/g@5.8 A/g	99.1%@5.8 A/g	400 cycles	19.9 W h/kg@1.58 kW/kg	43
NiCo-LDH/ZNO NR/CC	1 M KOH	604.2 F/g at 1 A/g	59.4%@20 A/g	5000 cycles		49
NiCO-LDH/ZnO NF/CC	1 M KOH	1577.6 F/g at 1 A/g	89.7%@20 A/g	5000 cycles	51.3 W h/kg@0.8 kW/kg	49
MnO_2@NF/NiFe-LDH	2 M KOH	4.27 F/cm^2@5 mA/cm^2	95.6%@15 mA/cm^2	1000 cycles	24.6 mW h/cm^2@350 mW/cm^2	78
NiMnCo-LDH@ZnO	6 M KOH	9.25 F/cm^2@2 mA/cm^2	87.5%@50 mA/cm^2	5000 cycles	24.6 W h/kg@0.170 kW/kg	79
ZnO@NiMn-LDH	**6 M KOH**	**569.3 F/g@1 A/g**	**76% after@100 mV/s**	**5000 cycles**	**16.08 W h/kg@0.798 kW/kg**	**this work**

is likely due to electrode activation, which enhances electrolyte ion access to the electrode material. After 1000 cycles, all the electrochemical sites of the electrode material become fully accessible to the electrolyte, thus stabilizing the capacitance.[72] Further EIS measurement of the fabricated ASC was measured before and after cycling in order to analyze capacitance decay over cycling as shown in Figure S5. The obtained Nyquist spectra consist small semicircle in the high frequency region with a slope in the low frequency region, and it is fitted with the equivalent circuit, as shown in the inset of Figure S5. The fitted equivalent circuit consists of series resistance (R_1), charge-transfer resistance (R_2), constant phase element (CPE_1), and Warburg impedance (W_1) related to the ionic diffusion. The increment in the series resistance from 0.67 to 1.57 Ω and charge transfer resistance from 0.14 to 1.9 Ω lead to the observed decrement in the specific capacitance over cycling. Additionally, a FESEM image of the positive electrode was taken after cycling, as shown in Figure S6. The morphology of ZnO@NiMn-LDH appears to be preserved, consisting of nanosheets (circled in yellow) along with amorphous nanoparticles, which is consistent with the observed cycling results and post cycling XRD results in Figure S3. The elemental mapping of a small area shows the presence of the constituent elements (Zn, Ni, Mn, and O), along with K, which originates from the electrolyte.

For comparison purposes, we have compared our findings with other ZnO and Ni-based LDH supercapacitor literature, as shown in Table 1.

4. CONCLUSIONS

In conclusion, this study investigated the electrochemical enhancement of ZnO through composite formation with various Ni-based layered double hydroxides (NiM′-LDHs), specifically NiMn-LDH, NiCo-LDH, and NiFe-LDH. The ZnO and ZnO@NiM′-LDH (M′ = Mn, Co, and Fe) composites were synthesized via a facile hydrothermal method. Among the tested composites, ZnO@NiMn-LDH exhibited superior electrochemical performance, achieving a specific capacitance of 569.3 F/g at a rate of 1 A/g. This is significantly higher compared to those of bare ZnO (5.9 times), ZnO@NiCo-LDH (2 times), and ZnO@NiFe-LDH (4.2 times). Additionally, the composite formation markedly improved the cyclic stability of ZnO from 23 to 76%. For a practical demonstration, an ASC was assembled using ZnO@NiMn-LDH as the positive electrode and AC as the negative electrode. This device delivered a specific capacitance of 45.22 F/g at a current rate of 1 A/g, energy density of 16.08 W h/kg at a power density of 798.8 W/kg, with a capacitance retention of 75% for 5000 cycles. The findings highlight the effectiveness of NiMn-LDH in enhancing the electrochemical properties of ZnO, paving the way for future advancements in supercapacitor applications.

■ ASSOCIATED CONTENT

Supporting Information

The Supporting Information is available free of charge at https://pubs.acs.org/doi/10.1021/acsnanoscienceau.4c00029.

FESEM image of ZnO@NiMn-LDH with EDS and elemental mapping (for Ni, Mn, Zn, and O), TEM image of ZnO@NiMn-LDH with SAED pattern, XRD spectra of the ZnO@NiMn-LDH electrode after cycling for 5000 cycles in 6 M KOH, specific capacitance variation of ZnO@NiMn-LDH//AC ASC at different current rates, fitted EIS of ZnO@NiMn-LDH//AC ASC before and after cycling with equivalent circuit, and FESEM image of the ZnO@NiMn-LDH electrode obtained from ASC after 5000 cycles with elemental mapping (for Ni, Mn, Zn, O, and K) (PDF)

https://doi.org/10.1021/acsnanoscienceau.4c00029
ACS Nanosci. Au 2024, 4, 399−408

AUTHOR INFORMATION

Corresponding Author

Kamlendra Awasthi − *Department of Physics, Malaviya National Institute of Technology Jaipur, Jaipur 302017 Rajasthan, India;* orcid.org/0000-0002-4407-1914; Email: kawasthi.phy@mnit.ac.in

Authors

Gaurav Pandey − *Department of Physics, Malaviya National Institute of Technology Jaipur, Jaipur 302017 Rajasthan, India*

Surendra Serawat − *Department of Physics, Malaviya National Institute of Technology Jaipur, Jaipur 302017 Rajasthan, India*

Complete contact information is available at: https://pubs.acs.org/10.1021/acsnanoscienceau.4c00029

Author Contributions

†G.P. and S.S. contributed equally. Awasthi Kamlendra: Conceptualization, supervision, resources, writing—review and editing, project administration, and funding acquisition. Pandey Gaurav: Data curation, formal analysis, investigation, and writing—original draft. Serwat Surendra: Data curation, formal analysis, investigation, and writing—original draft. CRediT: **Gaurav Pandey** conceptualization, data curation, formal analysis, investigation, methodology, writing - original draft, writing - review & editing; **Surendra Serawat** data curation, formal analysis, investigation, writing - original draft; **Kamlendra Awasthi** conceptualization, project administration, resources, supervision, writing - review & editing.

Notes

The authors declare no competing financial interest.

ACKNOWLEDGMENTS

The authors would like to thank MRC MNIT Jaipur for the characterization facilities.

REFERENCES

(1) Perera, F. Pollution from Fossil-Fuel Combustion is the Leading Environmental Threat to Global Pediatric Health and Equity: Solutions Exist. *Int. J. Environ. Res. Publ. Health* **2017**, *15*, 16.

(2) Whittingham, M. S. Lithium Batteries and Cathode Materials. *Chem. Rev.* **2004**, *104* (10), 4271−4302.

(3) Liu, C.; Bai, Y.; Li, W.; Yang, F.; Zhang, G.; Pang, H. In Situ Growth of Three-Dimensional MXene/Metal−Organic Framework Composites for High-Performance Supercapacitors. *Angew. Chem., Int. Ed.* **2022**, *61* (11), No. e202116282.

(4) Bai, Y.; Liu, C.; Chen, T.; Li, W.; Zheng, S.; Pi, Y.; Luo, Y.; Pang, H. MXene-Copper/Cobalt Hybrids via Lewis Acidic Molten Salts Etching for High Performance Symmetric Supercapacitors. *Angew. Chem., Int. Ed.* **2021**, *60* (48), 25318−25322.

(5) Zhou, H.; Zhu, G.; Dong, S.; Liu, P.; Lu, Y.; Zhou, Z.; Cao, S.; Zhang, Y.; Pang, H. Ethanol-Induced Ni^{2+}-Intercalated Cobalt Organic Frameworks on Vanadium Pentoxide for Synergistically Enhancing the Performance of 3D-Printed Micro-Supercapacitors. *Adv. Mater.* **2023**, *35* (19), No. e2211523.

(6) Abbas, N.; Shaheen, I.; Ali, I.; Ahmad, M.; Khan, S. A.; Qureshi, A.; Niazi, J. H.; Imran, M.; Lamiel, C.; Ansari, M. Z.; Hussain, I. Effect of Growth Duration of $Zn_{0.76}Co_{0.24}S$ Interconnected Nanosheets for High-Performance Flexible Energy Storage Electrode Materials. *Ceram. Int.* **2022**, *48* (23), 34251−34257.

(7) Abbas, N.; Shaheen, I.; Hussain, I.; Lamiel, C.; Ahmad, M.; Ma, X.; Qureshi, A.; Niazi, J. H.; Imran, M.; Ansari, M. Z.; Zhang, K. Glycerol-Mediated Synthesis of Copper-Doped Zinc Sulfide with Ultrathin Nanoflakes for Flexible Energy Electrode Materials. *J. Alloys Compd.* **2022**, *919*, 165701.

(8) Senthil, R. A.; Min, A.; Theerthagiri, J.; Kim, G.-A.; Choi, H. C.; Choi, M. Y. Insights on Ni-Based Layered Double Hydroxides for Electrochemical Supercapacitors: Underlying Aspects in Rational Design and Structural Evolution. *J. Energy Storage* **2023**, *72*, 108305.

(9) Gao, X.; Wang, P.; Pan, Z.; Claverie, J. P.; Wang, J. Recent Progress in Two-Dimensional Layered Double Hydroxides and Their Derivatives for Supercapacitors. *ChemSusChem* **2020**, *13* (6), 1226−1254.

(10) Yan, A.-L.; Wang, X.-C.; Cheng, J.-P. Research Progress of NiMn Layered Double Hydroxides for Supercapacitors: A Review. *Nanomaterials* **2018**, *8*, 747.

(11) He, X.; Zhang, X. A Comprehensive Review of Supercapacitors: Properties, Electrodes, Electrolytes and Thermal Management Systems Based on Phase Change Materials. *J. Energy Storage* **2022**, *56*, 106023.

(12) Zhong, C.; Deng, Y.; Hu, W.; Qiao, J.; Zhang, L.; Zhang, J. A Review of Electrolyte Materials and Compositions for Electrochemical Supercapacitors. *Chem. Soc. Rev.* **2015**, *44* (21), 7484−7539.

(13) Korkmaz, S.; Kariper, İ. A.; Karaman, O.; Karaman, C. The Production of RGO/RuO_2 Aerogel Supercapacitor and Analysis of Its Electrochemical Performances. *Ceram. Int.* **2021**, *47* (24), 34514−34520.

(14) Luo, Q.; Xu, P.; Qiu, Y.; Cheng, Z.; Chang, X.; Fan, H. Synthesis of ZnO Tetrapods for High-Performance Supercapacitor Applications. *Mater. Lett.* **2017**, *198*, 192−195.

(15) Dhas, S. D.; Maldar, P. S.; Patil, M. D.; Nagare, A. B.; Waikar, M. R.; Sonkawade, R. G.; Moholkar, A. V. Synthesis of NiO Nanoparticles for Supercapacitor Application as an Efficient Electrode Material. *Vacuum* **2020**, *181*, 109646.

(16) Liu, J.; Bao, J.; Zhang, X.; Gao, Y.; Zhang, Y.; Liu, L.; Cao, Z. MnO_2-Based Materials for Supercapacitor Electrodes: Challenges, Strategies and Prospects. *RSC Adv.* **2022**, *12* (55), 35556−35578.

(17) Xu, J.; Gao, L.; Cao, J.; Wang, W.; Chen, Z. Preparation and Electrochemical Capacitance of Cobalt Oxide (Co_3O_4) Nanotubes as Supercapacitor Material. *Electrochim. Acta* **2010**, *56* (2), 732−736.

(18) Ali, A.; Okba, B.; Salim, G.; Said, B. The Calculation of Band Gap Energy in Zinc Oxide Films. *J. Semicond.* **2015**, *36* (1), 13001.

(19) Pirhashemi, M.; Habibi-Yangjeh, A.; Rahim Pouran, S. Review on the Criteria Anticipated for the Fabrication of Highly Efficient ZnO-Based Visible-Light-Driven Photocatalysts. *J. Ind. Eng. Chem.* **2018**, *62*, 1−25.

(20) Borysiewicz, M. A. ZnO as a Functional Material, A Review. *Crystals* **2019**, *9* (10), 505.

(21) Ozgur, Ü.; Hofstetter, D.; Morkoç, H. ZnO Devices and Applications: A Review of Current Status and Future Prospects. *Proc. IEEE* **2010**, *98* (7), 1255−1268.

(22) Özgür, Ü.; Alivov, Y. I.; Liu, C.; Teke, A.; Reshchikov, M. A.; Doğan, S.; Avrutin, V.; Cho, S. J.; Morkoç, H. A Comprehensive Review of ZnO Materials and Devices. *J. Appl. Phys.* **2005**, *98* (4), 041301.

(23) Sharma, D. K.; Shukla, S.; Sharma, K. K.; Kumar, V. A Review on ZnO: Fundamental Properties and Applications. *Mater. Today: Proc.* **2022**, *49*, 3028−3035.

(24) Ahmad, M.; Yingying, S.; Nisar, A.; Sun, H.; Shen, W.; Wei, M.; Zhu, J. Synthesis of Hierarchical Flower-like ZnO Nanostructures and their Functionalization by Au Nanoparticles for Improved Photocatalytic and High Performance Li-Ion Battery Anodes. *J. Mater. Chem.* **2011**, *21* (21), 7723−7729.

(25) Guo, R.; Yue, W.; An, Y.; Ren, Y.; Yan, X. Graphene-Encapsulated Porous Carbon-ZnO Composites as High-Performance Anode Materials for Li-Ion Batteries. *Electrochim. Acta* **2014**, *135*, 161−167.

(26) Samuel, E.; Park, C.; Kim, T.; Joshi, B.; Aldalbahi, A.; Alanzi, H. S.; Swihart, M. T.; Yoon, W. Y.; Yoon, S. S. Dodecahedral ZnO/C Framework on Reduced Graphene Oxide Sheets for High-Performance Li-Ion Battery Anodes. *J. Alloys Compd.* **2020**, *834*, 155208.

(27) Jing, M.; Li, F.; Chen, M.; Long, F.; Wu, T. Binding ZnO Nanorods in Reduced Graphene Oxide via Facile Electrochemical Method for Na-Ion Battery. *Appl. Surf. Sci.* **2019**, *463*, 986−993.
(28) Wang, M.; Zhang, H.; Chen, C.; Zhao, H.; Li, L.; Lu, D.; Wang, J.; Huang, Y.; Ding, S. Zeolitic Imidazolate Framework-Derived ZnO Polyhedrons Wrapped by Co Nanoparticle Embedded in N-Doped Carbon for High-Performance Lithium and Potassium Storage. *J. Alloys Compd.* **2023**, *948*, 169677.
(29) Shaheen, I.; Ahmad, K. S.; Zequine, C.; Gupta, R. K.; Thomas, A. G.; Azad Malik, M. Sustainable Synthesis of Organic Framework-Derived ZnO Nanoparticles for Fabrication of Supercapacitor Electrode. *Environ. Technol.* **2022**, *43* (4), 605−616.
(30) Nagarani, S.; Sasikala, G.; Yuvaraj, M.; Kumar, R. D.; Balachandran, S.; Kumar, M. ZnO-CuO Nanoparticles Enameled on Reduced Graphene Nanosheets as Electrode Materials for Supercapacitors Applications. *J. Energy Storage* **2022**, *52*, 104969.
(31) Yue, H.; Shi, Z.; Wang, Q.; Cao, Z.; Dong, H.; Qiao, Y.; Yin, Y.; Yang, S. MOF-Derived Cobalt-Doped ZnO@C Composites as a High-Performance Anode Material for Lithium-Ion Batteries. *ACS Appl. Mater. Interfaces* **2014**, *6* (19), 17067−17074.
(32) Abinaya, C.; Prasankumar, T.; Jose, S. P.; Anitha, K.; Ekstrum, C.; Pearce, J. M.; Mayandi, J. Synthetic Method Dependent Physicochemical Properties and Electrochemical Performance of Ni-Doped ZnO. *ChemistrySelect* **2017**, *2* (28), 9014−9023.
(33) Brozek, C. K.; Zhou, D.; Liu, H.; Li, X.; Kittilstved, K. R.; Gamelin, D. R. Soluble Supercapacitors: Large and Reversible Charge Storage in Colloidal Iron-Doped ZnO Nanocrystals. *Nano Lett.* **2018**, *18* (5), 3297−3302.
(34) Ali, A.; Ammar, M.; Ali, M.; Yahya, Z.; Javaid, M. Y.; Hassan, S. U.; Ahmed, T. Mo-Doped ZnO Nanoflakes on Ni-Foam for Asymmetric Supercapacitor Applications. *RSC Adv.* **2019**, *9* (47), 27432−27438.
(35) Saranya, M.; Ramachandran, R.; Wang, F. Graphene-Zinc Oxide (G-ZnO) Nanocomposite for Electrochemical Supercapacitor Applications. *J. Sci.: Adv. Mater. Devices* **2016**, *1* (4), 454−460.
(36) Jayachandiran, J.; Yesuraj, J.; Arivanandhan, M.; Raja, A.; Suthanthiraraj, S. A.; Jayavel, R.; Nedumaran, D. Synthesis and Electrochemical Studies of RGO/ZnO Nanocomposite for Supercapacitor Application. *J. Inorg. Organomet. Polym. Mater.* **2018**, *28* (5), 2046−2055.
(37) Shaheen, I.; Hussain, I.; Zahra, T.; Memon, R.; Alothman, A. A.; Ouladsmane, M.; Qureshi, A.; Niazi, J. H. Electrophoretic Fabrication of ZnO/CuO and ZnO/CuO/RGO Heterostructures-Based Thin Films as Environmental Benign Flexible Electrode for Supercapacitor. *Chemosphere* **2023**, *322*, 138149.
(38) Zhao, Y.; Jiang, P. MnO_2 Nanosheets Grown on the ZnO-Nanorod-Modified Carbon Fibers for Supercapacitor Electrode Materials. *Colloids Surf., A* **2014**, *444*, 232−239.
(39) Wang, T.; Liu, J.; Ma, Y.; Han, S.; Gu, C.; Lian, J. P-N Heterojunction NiO/ZnO Electrode with High Electrochemical Performance for Supercapacitor Applications. *Electrochim. Acta* **2021**, *392*, 138976.
(40) Zhang, M.; Zang, R.; Zhang, M.; Liu, R.; Zhu, X.; Li, X.; Cui, H.; Zhu, H. Promoting the Cyclic and Rate Performance of Nickel Hydroxide with ZnO via Electrodeposition for Supercapacitor. *J. Alloys Compd.* **2022**, *911*, 164865.
(41) Shaheen, I.; Ahmad, K. S.; Zequine, C.; Gupta, R. K.; Thomas, A. G.; Malik, M. A. Green Synthesis of ZnO−Co_3O_4 Nanocomposite Using Facile Foliar Fuel and Investigation of its Electrochemical Behaviour for Supercapacitors. *New J. Chem.* **2020**, *44* (42), 18281−18292.
(42) Shaheen, I.; Ahmad, K. S.; Zequine, C.; Gupta, R. K.; Thomas, A. G.; Malik, M. A. Facile ZnO-Based Nanomaterial and its Fabrication as a Supercapacitor Electrode: Synthesis, Characterization and Electrochemical Studies. *RSC Adv.* **2021**, *11* (38), 23374−23384.
(43) Pang, H.; Ma, Y.; Li, G.; Chen, J.; Zhang, J.; Zheng, H.; Du, W. Facile Synthesis of Porous ZnO-NiO Composite Micropolyhedrons and their Application for High Power Supercapacitor Electrode Materials. *Dalton Trans.* **2012**, *41* (43), 13284−13291.
(44) Baig, M. M.; Gul, I. H.; Ahmad, R.; Baig, S. M.; Khan, M. Z.; Iqbal, N. One-Step Sonochemical Synthesis of NiMn-LDH for Supercapacitors and Overall Water Splitting. *J. Mater. Sci.* **2021**, *56* (33), 18636−18649.
(45) Arrabito, G.; Bonasera, A.; Prestopino, G.; Orsini, A.; Mattoccia, A.; Martinelli, E.; Pignataro, B.; Medaglia, P. G. Layered Double Hydroxides: A Toolbox for Chemistry and Biology. *Crystals* **2019**, *9*, 361.
(46) Wang, Q.; Wang, X. Regulating the Supercapacitor Properties of Hollow NiCo-LDHs via Morphology Engineering. *J. Alloys Compd.* **2023**, *937*, 168396.
(47) Ray, P. K.; Mohanty, R.; Parida, K. Recent Advancements of NiCo LDH and Graphene Based Nanohybrids for Supercapacitor Application. *J. Energy Storage* **2023**, *72*, 108335.
(48) Liao, F.; Zhao, X.; Yang, G.; Cheng, Q.; Mao, L.; Chen, L. Recent Advances on Two-Dimensional NiFe-LDHs and their Composites for Electrochemical Energy Conversion and Storage. *J. Alloys Compd.* **2021**, *872*, 159649.
(49) Xiong, H.; Liu, L.; Fang, L.; Wu, F.; Zhang, S.; Luo, H.; Tong, C.; Hu, B.; Zhou, M. 3D Self-Supporting Heterostructure NiCo-LDH/ZnO/CC Electrode for Flexible High-Performance Supercapacitor. *J. Alloys Compd.* **2021**, *857*, 158275.
(50) Chen, Y. B.; Ma, L. A.; Zhang, X.; Huang, L. K.; Chen, H. X.; Wang, Q. T. ZnO@NiCo-LDH Core-Shell Nanostructures Grown on Carbon Cloth for High-Performance Flexible Supercapacitor Electrodes. *Mater. Technol.* **2022**, *37* (9), 1146−1155.
(51) Hasnidawani, J. N.; Azlina, H. N.; Norita, H.; Bonnia, N. N.; Ratim, S.; Ali, E. S. Synthesis of ZnO Nanostructures Using Sol-Gel Method. *Procedia Chem.* **2016**, *19*, 211−216.
(52) Pudukudy, M.; Yaakob, Z. Facile Solid State Synthesis of ZnO Hexagonal Nanogranules with Excellent Photocatalytic Activity. *Appl. Surf. Sci.* **2014**, *292*, 520−530.
(53) Lee, S. D.; Nam, S.-H.; Kim, M.-H.; Boo, J.-H. Synthesis and Photocatalytic Property of ZnO Nanoparticles Prepared by Spray-Pyrolysis Method. *Phys. Procedia* **2012**, *32*, 320−326.
(54) Kumar, S.; Lawaniya, S. D.; Agarwal, S.; Yu, Y. T.; Nelamarri, S. R.; Kumar, M.; Mishra, Y. K.; Awasthi, K. Optimization of Pt Nanoparticles Loading in ZnO for Highly Selective and Stable Hydrogen Gas Sensor at Reduced Working Temperature. *Sens. Actuators, B* **2023**, *375*, 132943.
(55) Cheng, Y.; Wang, X.; Zhang, D.; Qiao, X.; Zhao, H.; Chang, L.; Yu, Z.; Xia, Y.; Fan, J.; Huang, C.; Yang, S. High-Capacity Binderless Supercapacitor Electrode Obtained from Sulfidation Large Interlayer Spacing of NiMn-LDH. *Electrochim. Acta* **2022**, *429*, 141039.
(56) Yang, H.; Ni, S.-Q.; Jiang, X.; Jiang, W.; Zhan, J. In Situ Fabrication of Single-Crystalline Porous ZnO Nanoplates on Zinc Foil to Support Silver Nanoparticles as a Stable SERS Substrate. *CrystEngComm* **2012**, *14* (18), 6023−6028.
(57) Zhang, B.; Yang, Y.; Cai, J.; Hou, X.; Yi, C.; Liao, X.; Liu, Y.; Chen, C.; Yu, D.; Zhou, X. Mg Doping of NiMn-LDH with a Three-Dimensional Porous Morphology for an Efficient Supercapacitor. *Dalton Trans.* **2023**, *52* (30), 10557−10566.
(58) Guo, X. L.; Liu, X. Y.; Hao, X. D.; Zhu, S. J.; Dong, F.; Wen, Z. Q.; Zhang, Y. X. Nickel-Manganese Layered Double Hydroxide Nanosheets Supported on Nickel Foam for High-Performance Supercapacitor Electrode Materials. *Electrochim. Acta* **2016**, *194*, 179−186.
(59) Das, J.; Pradhan, S. K.; Sahu, D. R.; Mishra, D. K.; Sarangi, S. N.; Nayak, B. B.; Verma, S.; Roul, B. K. Micro-Raman and XPS Studies of Pure ZnO Ceramics. *Physica B* **2010**, *405* (10), 2492−2497.
(60) Loh, J. Y. Y.; Kherani, N. P. X-ray Photospectroscopy and Electronic Studies of Reactor Parameters on Photocatalytic Hydrogenation of Carbon Dioxide by Defect-Laden Indium Oxide Hydroxide Nanorods. *Molecules* **2019**, *24*, 3818.
(61) Payne, B. P.; Biesinger, M. C.; McIntyre, N. S. Use of Oxygen/Nickel Ratios in the XPS Characterisation of Oxide Phases on Nickel Metal and Nickel Alloy Surfaces. *J. Electron Spectrosc. Relat. Phenom.* **2012**, *185* (5−7), 159−166.

https://doi.org/10.1021/acsnanoscienceau.4c00029
ACS Nanosci. Au 2024, 4, 399−408

(62) Jiang, T.; Wang, X.; Chen, J.; Mai, Y.; Liao, B.; Hu, W. Hierarchical Ni/Co-LDHs Catalyst for Catalytic Oxidation of Indoor Formaldehyde at Ambient Temperature. *J. Mater. Sci.: Mater. Electron.* **2020**, *31* (4), 3500−3509.
(63) Liu, Q.-Q.; Yue, K.-F.; Weng, X.-J.; Wang, Y.-Y. Luminescence Sensing and Supercapacitor Performances of a New (3,3)-Connected Cd-MOF. *CrystEngComm* **2019**, *21* (41), 6186−6195.
(64) Liu, Y.; Wang, Y.; Shi, C.; Chen, Y.; Li, D.; He, Z.; Wang, C.; Guo, L.; Ma, J. Co-ZIF Derived Porous NiCo-LDH Nanosheets/N Doped Carbon Foam for High-Performance Supercapacitor. *Carbon* **2020**, *165*, 129−138.
(65) Yao, S.; Zhang, Z.; Guo, S.; Yu, Z.; Zhang, X.; Zuo, P.; Wang, J.; Yin, G.; Huo, H. Hierarchical NiMn/NiMn-LDH/Ppy-C Induced by a Novel Phase-Transformation Activation Process for Long-Life Supercapacitor. *J. Colloid Interface Sci.* **2022**, *622*, 1020−1028.
(66) Rathore, H. K.; Hariram, M.; Awasthi, K.; Kumar, M.; Sarkar, D.; Ganesha, M. K.; Singh, A. K.; Das, D.; Shukla, A. Partially Carbonized Tungsten Oxide as Electrode Material for Asymmetric Supercapacitors. *J. Solid State Electrochem.* **2022**, *26* (9), 2039−2048.
(67) Wei, W.; Chen, Z.; Zhang, Y.; Chen, J.; Wan, L.; Du, C.; Xie, M.; Guo, X. Full-Faradaic-Active Nitrogen Species Doping Enables High-Energy-Density Carbon-Based Supercapacitor. *J. Energy Chem.* **2020**, *48*, 277−284.
(68) Kuang, H.; Zhang, H.; Liu, X.; Chen, Y.; Zhang, W.; Chen, H.; Ling, Q. Microwave-Assisted Synthesis of NiCo-LDH/Graphene Nanoscrolls Composite for Supercapacitor. *Carbon* **2022**, *190*, 57−67.
(69) Guo, Y.; Hong, X.; Wang, Y.; Li, Q.; Meng, J.; Dai, R.; Liu, X.; He, L.; Mai, L. Multicomponent Hierarchical Cu-Doped NiCo-LDH/CuO Double Arrays for Ultralong-Life Hybrid Fiber Supercapacitor. *Adv. Funct. Mater.* **2019**, *29* (24), 1809004.
(70) Rathore, H. K.; Hariram, M.; Ganesha, M. K.; Singh, A. K.; Das, D.; Kumar, M.; Awasthi, K.; Sarkar, D. Charge Storage Mechanism in Vanadium Telluride/Carbon Nanobelts as Electroactive Material in an Aqueous Asymmetric Supercapacitor. *J. Colloid Interface Sci.* **2022**, *621*, 110−118.
(71) Huang, J.; Yuan, K.; Chen, Y. Wide Voltage Aqueous Asymmetric Supercapacitors: Advances, Strategies, and Challenges. *Adv. Funct. Mater.* **2022**, *32* (4), 2108107.
(72) Rathore, H. K.; Hariram, M.; Ganesha, M. K.; Singh, A. K.; Das, D.; Kumar, M.; Awasthi, K.; Sarkar, D. Understanding Supercapacitive Performance of a N-Doped Vanadium Carbide/Carbon Composite as an Anode Material in an all Pseudocapacitive Asymmetric Cell. *Sustain. Energy Fuels* **2023**, *7* (11), 2613−2626.
(73) Ranjithkumar, R.; Arasi, S. E.; Sudhahar, S.; Nallamuthu, N.; Devendran, P.; Lakshmanan, P.; Kumar, M. K. Enhanced Electrochemical Studies of ZnO/CNT Nanocomposite for Supercapacitor Devices. *Physica B* **2019**, *568*, 51−59.
(74) Kumar, R. D.; Nagarani, S.; Balachandran, S.; Brundha, C.; Kumar, S. H.; Manigandan, R.; Kumar, M.; Sethuraman, V.; Kim, S. H. High Performing Hexagonal-Shaped ZnO Nanopowder for Pseudo-Supercapacitors Applications. *Surf. Interfaces* **2022**, *33*, 102203.
(75) Rai, S.; Bhujel, R.; Khadka, M.; Chetry, R. L.; Swain, B. P.; Biswas, J. Synthesis, Characterizations, and Electrochemical Studies of ZnO/Reduced Graphene Oxide Nanohybrids for Supercapacitor Application. *Mater. Today Chem.* **2021**, *20*, 100472.
(76) Sivakumar, S.; Robinson, Y.; Mala, N. A. Studies on Photocatalytic Performance and Supercapacitor Applications of Undoped and Cu-Doped ZnO Nanoparticles. *Appl. Surf. Sci. Adv.* **2022**, *12*, 100344.
(77) Tourchi Moghadam, M. T.; Seifi, M. Fabrication and Investigation of ZnO-CNT@Fe_3O_4/NF as Supercapacitor Electrode by Using a Novel Preparation Method of CNT. *Diam. Relat. Mater.* **2022**, *125*, 108962.
(78) Li, M.; Zhou, M.; Wen, Z. Q.; Zhang, Y. X. Flower-like NiFe Layered Double Hydroxides Coated MnO_2 for High-Performance Flexible Supercapacitors. *J. Energy Storage* **2017**, *11*, 242−248.
(79) Zhang, A.; Zhang, Q.; Huang, J.; Fu, H.; Zong, H.; Guo, H. NiMnCo-LDH In-Situ Derived from ZIF-67@ZnO as Self-Supporting Electrode for Asymmetric Supercapacitor Device. *Chem. Eng. J.* **2024**, *487*, 150587.

https://doi.org/10.1021/acsnanoscienceau.4c00029
ACS Nanosci. Au 2024, 4, 399−408